Adiabatic spin dynamics from spin-density-functional theory: Application to Fe, Co, and Ni

S. V. Halilov and H. Eschrig
Institut für Theoretische Physik, TU Dresden, D-01062 Dresden, Germany

A. Y. Perlov*
Max-Planck-Institut für Physik Komplexer Systeme, D-01069 Dresden, Germany

P. M. Oppeneer
Institut für Theoretische Physik, TU Dresden, D-01062 Dresden, Germany

(Received 2 February 1998)

The adiabatic theory of spin-density waves is developed on the basis of spin-density-functional theory. The wave-number-dependent exchange constant matrix is obtained from spin-density-functional calculations with constrained moment directions. The central assumption considers a fast electronic and a slow magnetic time scale, and postulates negligible correlation of the fast motion between different ionic sites. The parameter-free calculated magnon spectra for Fe, Co, and Ni are in excellent agreement with available experimental data. In the case of Fe, they show strong Kohn anomalies. Using Planck statistics at low temperature, the temperature dependence of the magnetization is well described up to half the Curie temperature. It is conjectured that correlated local-moment clusters survive the Curie transition. On this basis, calculated Curie temperatures are obtained within 10% deviation from experiment for Fe and Co, but 30% to low for Ni.
[S0163-1829(98)04425-7]

I. INTRODUCTION

Spin-density-functional theory (SDFT) in local spin-density approximation (LSDA) and beyond has proved over the years to yield reliable results for the ground state of large classes of magnetic materials with collinear[1–3] and noncollinear[4,5] spin alignment. Attempts of extensions to the description of magnetic low-energy excitations and of the thermodynamic state rest on an adiabatic understanding of a slow moment motion in a fast electronic medium. The disordered local-moment approach[6–9] and the spin spiral energy functional approach[10,11] employ Green's functions and band-structure techniques, respectively, to develop a notion of local moments interacting with effective exchange forces out of an itinerant electron situation. Equation of motion and molecular-dynamics approaches[12–14] rest on similar adiabaticity ideas. Besides, more general nonadiabatic theories pointed to the importance of low-energy transversal excitations for the magnetic phase diagram (for reviews, see Refs. 15 and 16). In Ref. 17, the present authors adopted an approach close to that of Refs. 10 and 11 but put focus on small amplitude spin spirals instead of the 90° spirals considered in the latter work in order to study magnon dynamics in more detail. The results indicate that in the case of the elemental $3d$ ferromagnets 90° spirals with short wavelength are irrelevant even at the Curie transition. Furthermore, we do not include the intra-atomic energy terms in the adiabatic Hamiltonian.

The aim of the present paper is on the one hand to make our approach as explicit as possible, and, on the other hand, to present all the important numerical results obtained for the ferromagnetic $3d$ metals. In particular, we obtain all relevant exchange constants from the total-energy surface in the vicinity of the ordered magnetic ground state, i.e., for small spin spiral amplitudes. Our focus is on adiabatic magnon dynamics. However, it turns out that the same phase space is relevant for the quasiclassical disordered moment dynamics at the Curie transition.

It must be emphasized that the adiabatic magnon spectrum is a coarsened excitation spectrum with fast individual electron spin-flip degrees of freedom integrated out. The alternative approach[18–22] via the transverse dynamical susceptibility $\chi^{-+}(\boldsymbol{q},\omega)$ does not rest on the adiabatic approximation and hence is able to describe both the magnon dispersion and the interband spin-flip continuum as well as their interference. On the other hand, the adiabatic approach yields the magnon stiffness with the same accuracy, but in addition yields all the details of far reaching exchange interactions, manifesting, e.g., in Kohn anomalies.

The paper is organized as follows. In the next section we give a full self-contained description of the adiabatic spin dynamics. For the sake of clarity we start with defining the lattice site spin moment, and then derive the Fourier transformed exchange constants directly from SDFT spin spiral results for small amplitudes. This is followed by a discussion of central assumptions of the adiabatic approach leading to the equations of motion of the Landau-Lifshits-type for the moments. Linearization and quantization results in the description of adiabatic magnon spectra for arbitrary crystals with collinear magnetic order. In Sec. III we analyze moment behavior and exchange interactions for the ferromagnetic $3d$ metals, present their adiabatic magnon spectra, and analyze the appearance of Kohn anomalies in Fe and their origin. In Sec. IV we apply the adiabatic magnon dynamics with Planck statistics to treat low-temperature thermodynamics. For $3d$ metals, the magnetization vs temperature curves are very close to experiment up to about half the Curie temperature. We use our calculated exchange constants for a quasi-

classical mean-field treatment of the thermodynamics around the transition to magnetic order. The transition temperatures compare well with results of disordered local-moment approaches.

II. ADIABATIC SPIN DYNAMICS

A. Lattice site spin magnetic moment

Recall that since the particle spin operator commutes with the particle position operator in quantum theory, there is a well-defined operator of vector spin density as a function of space coordinate $\boldsymbol{r}$ and time t:

$$\hat{\boldsymbol{\sigma}}(\boldsymbol{r},t)=\frac{1}{2}\sum_{ss'}\ \hat{\psi}_s^{\dagger}(\boldsymbol{r},t)\boldsymbol{\sigma}_{ss'}\hat{\psi}_{s'}(\boldsymbol{r},t). \tag{2.1}$$

Here, $\hat{\psi}_s$ is the s component of the spinor-field operator in the Heisenberg picture, and $\boldsymbol{\sigma}=(\sigma^x,\sigma^y,\sigma^z)$ are the Pauli matrices. The expectation value of vector spin density is

$$\boldsymbol{\sigma}(\boldsymbol{r},t)=\langle\hat{\boldsymbol{\sigma}}(\boldsymbol{r},t)\rangle=\tfrac{1}{2}\ \mathrm{tr}\ (n(\boldsymbol{r},t)\boldsymbol{\sigma}), \tag{2.2}$$

where $n(\boldsymbol{r},t)$ is the spin-density matrix

$$n_{ss'}(\boldsymbol{r},t)=\langle\hat{\psi}_{s'}^{\dagger}\hat{\psi}_s\rangle \tag{2.3}$$

and tr means the trace with respect to spin indices.

Given a partitioning of the total crystal volume V into disjunct cell volumes V_i around lattice sites i:

$$V=\cup_i V_i,\quad V_i\cap V_j=0\ \text{ for }\ i\neq j, \tag{2.4}$$

the operator of the lattice site spin magnetic moment is naturally defined as

$$\hat{\boldsymbol{M}}_i(t)=-g\mu_{\mathrm{Bohr}}\int_{V_i}\hat{\boldsymbol{\sigma}}(\boldsymbol{r},t)d^3r, \tag{2.5}$$

and its expectation value is

$$\boldsymbol{M}_i(t)=\langle\hat{\boldsymbol{M}}_i(t)\rangle=-\frac{g\mu_{\mathrm{Bohr}}}{2}\ \mathrm{tr}\left(\boldsymbol{\sigma}\int_{V_i}n(\boldsymbol{r},t)d^3r\right). \tag{2.6}$$

Here, $-g\mu_{\mathrm{Bohr}}/2$ is the spin magnetic moment of a free electron. [In Ref. 17 the same operator (2.5) was introduced in an alternative representation.]

From Eqs. (2.1), (2.4), and (2.5) the equal-time commutation relations

$$[\hat{M}_{i\alpha},\hat{M}_{j\beta}]_-=-ig\mu_{\mathrm{Bohr}}\delta_{ij}\epsilon_{\alpha\beta\gamma}\hat{M}_{i\gamma} \tag{2.7}$$

are staightforwardly obtained, where $\alpha\beta\gamma$ are Cartesian indices, and $\epsilon_{\alpha\beta\gamma}$ is the fundamental three-form (antisymmetric tensor). These relations hold independent of itineracy or locality.

By way of contrast, a lattice site orbital moment cannot be defined properly unless the orbitals are strictly localized and nonoverlapping. The noncommutativity of the operators of particle orbital moment and of particle position prevents the existence of an unambiguous orbital moment density.

B. Spin-density-functional calculation with constrained moment directions

SDFT provides a tool to calculate the total energy and the spin-density matrix (2.3) of the ground state in a crystal (with fixed ion sites). If the ground state is spin polarized, this calculation hence yields the (stationary) expectation values of the site spin magnetic moment vectors (2.6), too. The spin-density matrix is obtained as

$$n_{ss'}(\boldsymbol{r})=\sum_{\boldsymbol{k}n}^{\mathrm{occ.}}\ \phi_{\boldsymbol{k}n}(\boldsymbol{r},s)\,\phi_{\boldsymbol{k}n}^{*}(\boldsymbol{r},s') \tag{2.8}$$

from the Kohn-Sham spin orbitals $\phi_{\boldsymbol{k}n}(\boldsymbol{r},s)$ of Bloch states $\boldsymbol{k}n$ corresponding to Kohn-Sham orbital energies $\epsilon_{\boldsymbol{k}n}$ below the Fermi level.

The 2×2 matrix (2.8) may be diagonalized by an $\boldsymbol{r}$-dependent 2×2 unitary $U(\boldsymbol{r})$:

$$U(\boldsymbol{r})n(\boldsymbol{r})U^{\dagger}(\boldsymbol{r})=\mathrm{diag}[n_{\uparrow}(\boldsymbol{r}),n_{\downarrow}(\boldsymbol{r})]. \tag{2.9}$$

If the vector spin density at position $\boldsymbol{r}$ points into a direction that has a polar angle θ and an azimuth angle ϕ with the global xyz coordinate system, then

$$U=\begin{pmatrix}\cos\theta/2\exp-i\phi/2 & \sin\theta/2\exp i\phi/2\\ \sin\theta/2\exp i\phi/2 & -\cos\theta/2\exp-i\phi/2\end{pmatrix}. \tag{2.10}$$

In LSDA, the effective Kohn-Sham potential $v(\boldsymbol{r})$ is diagonal together with the spin-density matrix, and its diagonal entries at position $\boldsymbol{r}$ are explicitly calculated from the two numbers $n_{\uparrow}(\boldsymbol{r}),n_{\downarrow}(\boldsymbol{r})$. The resulting diagonal $v(\boldsymbol{r})$ may be rotated back to the global coordinate system by means of the unitary $U^{\dagger}(\boldsymbol{r})$, into a full spin matrix $v_{ss'}(\boldsymbol{r})$, and inserted into the Kohn-Sham equation for the next self-consistency cycle. The potential matrix $v_{ss'}(\boldsymbol{r})$ and the spin-density matrix $n_{ss'}(\boldsymbol{r})$ recalculated in the next iteration cycle are not simultaneously diagonal, unless self-consistency is reached.

In practical implementations[4,5] one assumes the unitary $U(\boldsymbol{r})$ to be constant in each lattice site volume V_i and fixes the angles θ_i and ϕ_i at predefined values for each lattice site separately. Then one attains self-consistency under these constrained moment directions and finds the magnitude $|\boldsymbol{M}_i|$ of the spin magnetic moment at each lattice site and the total energy corresponding to this magnetic configuration with predefined moment directions. In a second step, one then searches for that moment configuration that yields the minimum of the total energy. As long as spin-orbit coupling can be neglected, the position-dependent spin rotation $U(\boldsymbol{r})$ does not affect the orbital operation of the Kohn-Sham Hamiltonian.[23] Transformation of the spinor factor of the Kohn-Sham orbitals by $U(\boldsymbol{r})$ diagonalizes the Kohn-Sham Hamiltonian and retains the full crystal symmetry in each diagonal. Spin and orbital degrees of freedom are on this level of description coupled only via the common Fermi level in Eq. (2.8) and via the LSDA expression of the potential through the spin-density matrix.

A priori, there is no justification to assume $U(\boldsymbol{r})$ constant inside each lattice site volume. There is, however, a large body of successful calculations of magnetic structures this way.

To cover the full phase space of spin configurations, it would in a Fourier representation be necessary to introduce two independent wave vectors for the position dependence of θ and ϕ. Since, however, in linear spin-wave modes θ is constant, we keep it constant on each sublattice ν (if there are several sublattices) and consider only configurations

$$\boldsymbol{M}_i = M_i(\sin\theta_i\cos\phi_i, \sin\theta_i\sin\phi_i, \cos\theta_i), \quad (2.11a)$$

$$\theta_i = \theta_\nu, \quad \phi_i = \boldsymbol{q}\cdot\boldsymbol{R}_i + \phi_\nu. \quad (2.11b)$$

Then, the modulus of the spin magnetic moment and the total energy (per unit cell) are obtained as functions $M_\nu(\theta_\mu, \phi_\mu, \boldsymbol{q}), E(\theta_\mu, \phi_\mu, \boldsymbol{q})$.

Our goal is to represent the total energy in the form

$$\begin{aligned} E &= E_0(M_i^2) - \frac{1}{2N}\sum_{i\neq j} J_{ij}\boldsymbol{M}_i\cdot\boldsymbol{M}_j + \cdots \\ &= E_0(M_i^2) - \frac{1}{2N}\sum_{i\neq j} J_{ij}M_iM_j \\ &\quad \times[\cos\theta_i\cos\theta_j + \sin\theta_i\sin\theta_j\cos(\phi_i - \phi_j)] + \cdots \end{aligned} \quad (2.12)$$

where N is the number of unit cells in the crystal and higher than second-order terms in the angles θ are omitted. We introduce an index notation

$$\boldsymbol{R}_i = \boldsymbol{R} + \boldsymbol{\tau}_\nu = \boldsymbol{R}_{[\nu+\boldsymbol{R}]}, \quad [\nu+0] \equiv \nu, \quad (2.13)$$

where $\boldsymbol{R}$ is a lattice period and $\boldsymbol{\tau}_\nu$ is a basis vector of the unit cell, and define the Fourier transform of the exchange constants J_{ij} to be

$$J_{\boldsymbol{q}}^{\mu\nu} = \delta_{\mu\nu}J_{\mu\mu} - \sum_{\boldsymbol{R}} J_{\mu[\nu+\boldsymbol{R}]}e^{i\boldsymbol{q}(\boldsymbol{\tau}_\mu - \boldsymbol{\tau}_\nu - \boldsymbol{R})}. \quad (2.14)$$

In Eq. (2.12), the J_{ij} may be chosen real, symmetric, $J_{ij} = J_{ji}$, and lattice periodic, $J_{[\mu+\boldsymbol{R}][\nu+\boldsymbol{R}]} = J_{\mu\nu}$. Hence, from Eq. (2.14) the symmetry relations

$$J_{\boldsymbol{q}}^{\mu\nu} = J_{-\boldsymbol{q}}^{\nu\mu}, \quad \mathrm{Re}J_{\boldsymbol{q}}^{\mu\nu} = \mathrm{Re}J_{-\boldsymbol{q}}^{\mu\nu}, \quad \mathrm{Im}J_{\boldsymbol{q}}^{\mu\nu} = -\mathrm{Im}J_{-\boldsymbol{q}}^{\mu\nu} \quad (2.15)$$

follow. For a collinear ferromagnetic ground state and small θ, we have from Eq. (2.12)

$$\begin{aligned} E &= E_0 + \frac{1}{2}\sum_{\mu\nu} M_\mu M_\nu[(1 - \theta_\mu^2/2 - \theta_\nu^2/2)J_0^{\mu\nu} \\ &\quad + \theta_\mu\theta_\nu\mathrm{Re}(J_{\boldsymbol{q}}^{\mu\nu}e^{i(\phi_\mu - \phi_\nu)})] + \cdots \end{aligned} \quad (2.16)$$

and hence

$$\mathrm{Re}J_{\boldsymbol{q}}^{\mu\nu} - \delta_{\mu\nu}\sum_\lambda \frac{M_\lambda}{M_\mu}J_0^{\lambda\mu} = \left[\frac{1}{M_\mu M_\nu}\frac{\partial^2 E}{\partial\theta_\mu\partial\theta_\nu}\right]_{\theta=0;\,\phi_\mu - \phi_\nu = 0}, \quad (2.17a)$$

$$\mathrm{Im}J_{\boldsymbol{q}}^{\mu\nu} = \left[\frac{1}{M_\mu M_\nu}\frac{\partial^2 E}{\partial\theta_\mu\partial\theta_\nu}\right]_{\theta=0;\,\phi_\mu - \phi_\nu = \pi/2}, \quad \mu \neq \nu. \quad (2.17b)$$

From Eq. (2.15), clearly $\mathrm{Im}J_{\boldsymbol{q}}^{\mu\mu} = 0$, and later on we will only need

$$\tilde{J}_{\boldsymbol{q}}^{\mu\nu} = J_{\boldsymbol{q}}^{\mu\nu} - \delta_{\mu\nu}\sum_\lambda \frac{M_\lambda}{M_\mu}J_0^{\lambda\mu}. \quad (2.18)$$

In this way, the Fourier transforms of the exchange constants, $\tilde{J}_{\boldsymbol{q}}^{\mu\nu}$ for each $\boldsymbol{q}$ are directly obtained from total-energy calculations for a few spin spirals (2.11b) at that wave vector $\boldsymbol{q}$. By analogy with the frozen phonon approach to the calculation of lattice dynamics the above approach to the calculation of Eq. (2.18) can be referred to as a ''frozen magnon'' approach. Moreover, as long as one neglects spin-orbit coupling, the frozen magnon calculation is much simpler compared to frozen phonon calculations because the former does not call for large superstructure cells and commensurability.

C. Adiabatic spin-wave Hamiltonian

The time scale of the magnetic moment dynamics in a solid is much larger than the time scale of electrons orbiting around an atom and even larger than a/v_F, the lattice spacing over the Fermi velocity, which is the time scale of motion of a Bloch electron through the crystal (typical magnon energies for a transition metal are a few tenths of an eV while the d-band width is a few eV). Nevertheless, a systematic adiabatic approach has not been developed for this situation, simply because there is no large mass governing this time scale. However, on a heuristic level, the above described frozen magnon approach can be given a physical meaning. Suppose that an additional *external* potential $v_{ss'}(\boldsymbol{r})$ is applied that enforces the *ground-state* spin-density matrix to attain the values corresponding to our constrained-moment-directions result. Then, the corresponding energy (2.12) is the internal energy of that ground state, that is, the energy not counting the interacton energy with that additional external potential $v_{ss'}(\boldsymbol{r})$.

If we now allow this external potential to slowly vary in time, we may have an adiabatic situation

$$\langle\hat{\boldsymbol{M}}_i(t)\rangle \approx \langle\hat{\boldsymbol{M}}_i\rangle_{\mathrm{fast}}(t), \quad (2.19)$$

where on the left the average is taken with the true nonstationary state while on the right the average is with ground states of the fast electronic motion, parametrically depending on time.

An itinerant system is never in an eigenstate of $\hat{\boldsymbol{M}}_i^2$, that is, generally

$$\langle\hat{\boldsymbol{M}}_i^2\rangle \neq \langle\hat{\boldsymbol{M}}_i\rangle^2. \quad (2.20)$$

However, our central assumption will be

$$\langle\hat{\boldsymbol{M}}_i\cdot\hat{\boldsymbol{M}}_j\rangle_{\mathrm{fast}} \approx \langle\hat{\boldsymbol{M}}_i\rangle_{\mathrm{fast}}\cdot\langle\hat{\boldsymbol{M}}_j\rangle_{\mathrm{fast}} = \boldsymbol{M}_i\cdot\boldsymbol{M}_j \quad \text{for } i \neq j, \quad (2.21)$$

where the average is over parametrically time-dependent ground states of the fast electronic motion: *we assume the relevant electronic correlation hole to be essentially in the inner part of the atomic volume.*

We aim at introducing an adiabatic Hamiltonian

$$\hat{H}_{\mathrm{ad}} = -\frac{1}{2}\sum_{i\neq j} J_{ij}\hat{\boldsymbol{M}}_i\cdot\hat{\boldsymbol{M}}_j + \cdots \tag{2.22}$$

corresponding to the electronic ground-state energies E from Eq. (2.12):

$$\langle \hat{H}_{\mathrm{ad}}\rangle_{\mathrm{fast}} = N(E-E_0). \tag{2.23}$$

On account of our central assumption (2.21), this will be the case, if the exchange constants in Eqs. (2.12) and (2.22) are the same.

The Heisenberg equations of motion

$$-i\hbar\frac{d\hat{\boldsymbol{M}}_i}{dt} = [\hat{H}_{\mathrm{ad}},\hat{\boldsymbol{M}}_i]_- \tag{2.24}$$

for the magnetic moment operator are now easily obtained from Eq. (2.7), and their adiabatic quantum average leads via using Eq. (2.19) on the left-hand side and Eq. (2.21) on the right-hand side to the Landau-Lifshits-type equations

$$\frac{dM_i}{dt} = 0, \tag{2.25a}$$

$$\sin\theta_i\frac{d\phi_i}{dt} = -\frac{g\mu_{\mathrm{Bohr}}}{\hbar}\sum_{j(\neq i)} J_{ij}M_j \times[\cos\theta_i\sin\theta_j\cos(\phi_i-\phi_j)-\sin\theta_i\cos\theta_j], \tag{2.25b}$$

$$\frac{d\theta_i}{dt} = -\frac{g\mu_{\mathrm{Bohr}}}{\hbar}\sum_{j(\neq i)} J_{ij}M_j\sin\theta_i\sin(\phi_i-\phi_j), \tag{2.25c}$$

which under the assumptions (2.19) and (2.21) are valid for all wave vectors $\boldsymbol{q}$ rather than only in the long-wavelength (hydrodynamic) limit.

Note that Eq. (2.25a) follows since $\hat{\boldsymbol{M}}_i^2$ commutes with all $\hat{\boldsymbol{M}}_j$; for this reason we need also not include the E_0 term in Eq. (2.22). Longitidinal moment dynamics is nonadiabatic in our approach to this type of adiabaticity. It is governed by individual electronic spin flips like Stoner excitations, which are fast in our understanding. The numerical results for transition metals presented in the next section will support this picture. Note further that magnetic anisotropy terms from crystal fields or from spin-orbit coupling can easily be incorporated by adding anisotropic terms to Eq. (2.22).

D. Linearization and quantization

If $\theta \ll 1$, the equations of motion (2.25) imply immediately $d\theta/dt \approx 0$, $d\phi/dt \approx \omega = \mathrm{const}$, and in lowest order we are left with

$$\theta_i\omega = -\frac{g\mu_{\mathrm{Bohr}}}{\hbar}\sum_{j(\neq i)} J_{ij}M_j[\theta_j\cos(\phi_i-\phi_j)-\theta_i]. \tag{2.26}$$

Specifying $i=\mu$, $j=[\nu+\boldsymbol{R}]$, and

$$\phi_j = \omega t + \boldsymbol{q}\cdot(\boldsymbol{R}+\boldsymbol{\tau}_\nu)+\phi_\nu, \tag{2.27}$$

Eq. (2.26) is, on account of Eq. (2.14), cast into

$$\theta_\mu e^{i\phi_\mu}\omega = \frac{g\mu_{\mathrm{Bohr}}}{\hbar}\sum_\nu M_\nu\theta_\nu e^{i\phi_\nu} \times\left(J_{\boldsymbol{q}}^{\mu\nu}-\delta_{\mu\nu}\sum_\lambda\frac{M_\lambda}{M_\mu}J_0^{\mu\lambda}\right). \tag{2.28}$$

This is a linear eigenvalue problem with eigenvalue ω and eigenvector

$$\vartheta_\mu = \sqrt{M_\mu}\theta_\mu e^{i\phi_\mu}, \tag{2.29}$$

and in order to yield real eigenvalues $\omega_{\boldsymbol{q}n}$ (with branch index n) the matrix in large parentheses must be Hermitian, which is true as seen from Eq. (2.15). The final eigenvalue problem is

$$\vartheta_{\mu\boldsymbol{q}n}\omega_{\boldsymbol{q}n} = \frac{g\mu_{\mathrm{Bohr}}}{\hbar}\sum_\nu \tilde{J}_{\boldsymbol{q}}^{\mu\nu}\vartheta_{\nu\boldsymbol{q}n}. \tag{2.30}$$

Its solutions together with Eq. (2.29) yield the adiabatic spin-wave modes $(\theta_{\mu\boldsymbol{q}n},\phi_{\mu\boldsymbol{q}n})$ and their frequencies $\omega_{\boldsymbol{q}n}$.

Equation (2.18) together with the first relation (2.15) implies

$$\sum_\nu \tilde{J}_0^{\mu\nu}M_\nu = 0. \tag{2.31}$$

As immediately seen from Eqs. (2.30) and (2.29), this expresses the acoustical sum rule for a general crystal, yielding for $\boldsymbol{q}=0$ the zero frequency mode $\theta_\mu=\mathrm{const}$, $\phi_\mu=\mathrm{const}$ with lattice site-independent constants. It originates from our energy expression (2.12) not containing anisotropic terms.

If we put back the spin-wave mode into the energy expression (2.16), we obtain its energy that should be equal to $\hbar\omega_{\boldsymbol{q}n}$ for one magnon:

$$\frac{N}{2}\sum_{\mu\nu} e^{-i\phi_{\mu\boldsymbol{q}n}}\theta_{\mu\boldsymbol{q}n}M_\mu\tilde{J}_{\boldsymbol{q}}^{\mu\nu}M_\nu\theta_{\nu\boldsymbol{q}n}e^{i\phi_{\nu\boldsymbol{q}n}} \overset{!}{=} \hbar\omega_{\boldsymbol{q}n}. \tag{2.32}$$

The left-hand side of this condition equals the result of multiplying Eq. (2.30) by $(N/2)(\hbar/g\mu_{\mathrm{Bohr}})\vartheta^*_{\mu\boldsymbol{q}n}$ and summing over μ. Hence, the final quantization condition is

$$\frac{N}{2g\mu_{\mathrm{Bohr}}}\sum_\mu M_\mu\theta^2_{\mu\boldsymbol{q}n} = 1. \tag{2.33}$$

This relation quantizes the spin-wave amplitude $\theta_{\mu\boldsymbol{q}n}$ and will become essential in applications to statistics at nonzero temperature in Sec. IV.

III. CALCULATED ZERO-TEMPERATURE SPIN DYNAMICS OF TRANSITION METALS

In this section we analyze how the approach developed in the last section applies to the ferromagnetic $3d$ metals bcc-Fe, fcc- and hcp-Co, and fcc-Ni. Except for hcp-Co, these are weakly anisotropic ferromagnets, and we apply the expressions of last section without modification due to anisotropy. A linear-muffin-tin-orbital method[24] in scalar relativistic approximation (neglect of spin-orbit coupling)[25] is used for the frozen magnon calculations. The LSDA parametrization due

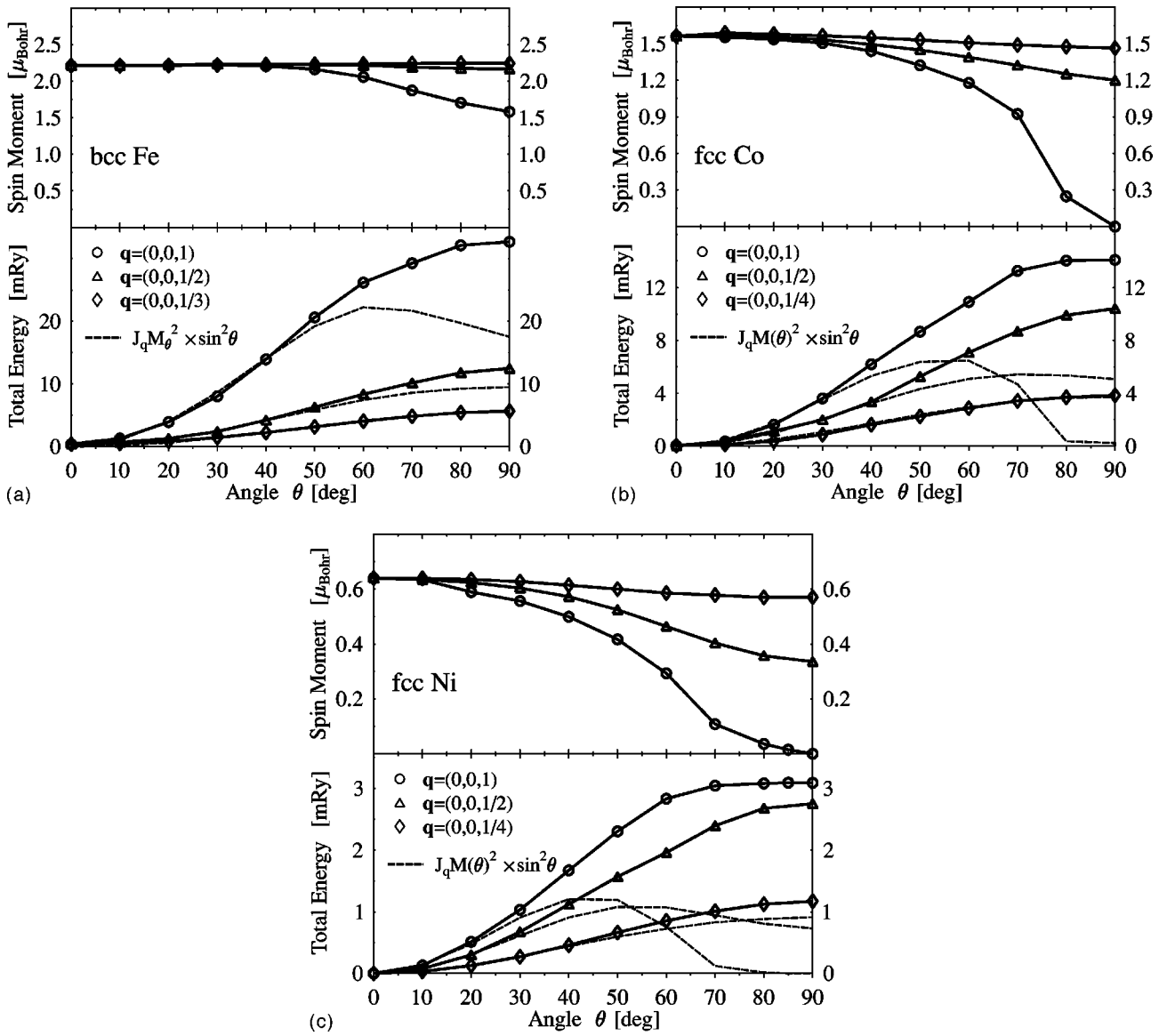

FIG. 1. Site spin moment $M(\theta,\boldsymbol{q})$ and total energy $\Delta E(\theta,\boldsymbol{q})=E(\theta,\boldsymbol{q})-E(0,0)$ as functions of θ for spin spirals with $\boldsymbol{q}=(0,0,\frac{1}{4}),(0,0,\frac{1}{2}),(0,0,1)$ in units of π/a. Symbols mark calculated values and solid lines are guides for the eye. The dashed lines correspond to functions $JM^2(\theta)\sin^2\theta$ for fixed $\boldsymbol{q}$. (a) bcc-Fe, (b) fcc-Co, (c) fcc-Ni.

to von Barth and Hedin[26] of the spin-density functional has been used.

A. Validity of the energy expression and moment behavior

In the case of a Bravais lattice as bcc or fcc, the energy expression (2.12) (for arbitrary θ) simplifies to

$$E-E_0=\frac{M^2}{2}[J_0\cos^2\theta+J_{\boldsymbol{q}}\sin^2\theta]=\frac{M^2}{2}[J_0+\tilde{J}_{\boldsymbol{q}}\sin^2\theta]. \tag{3.1}$$

Independent SDFT calculations of $M(\theta,\boldsymbol{q}),E(\theta,\boldsymbol{q})$ for various constrained spin spiral configurations have been performed to test the validity of expression (3.1) and to analyze the behavior of $M(\theta,\boldsymbol{q})$. The results are presented in Fig. 1.

What is most striking about these results is the remarkable stability of the site moment M, particularly for bcc-Fe. The moment is considerably reduced only if both $\boldsymbol{q}$ and θ are large: only if large $\boldsymbol{q}$ (and hence large $\omega_{\boldsymbol{q}}$) magnons have occupation numbers $\sim N$ (that is, ~ 1 per site), they induce longitidinal spin fluctuations and reduce the moment. That longitudinal magnetization density waves should have higher energies than transversal ones has been repeatedly stated in the literature.[27,28] It is particularly this stability of the moment that justifies the whole approach of the last section, above all, Eq. (2.21).

The comparison of the calculated values of $\Delta E(\theta)$ of Fig. 1 with the $M^2(\theta)\sin^2\theta$ curves according to Eq. (3.1) gives strong support to the use of the energy expression (2.12) and hence to the relevance of the exchange constant matrix (2.17) and (2.18), as long as not both θ and $\boldsymbol{q}$ are simultaneously large. On the other hand, it also indicates that the exchange constants $J_{\boldsymbol{q}}$ should not be determined from $\theta=90°$ spin spirals.

Figure 2 shows the individual contributions to $\Delta E(\theta)$ for Ni as an example. As is seen, the total energy follows essen-

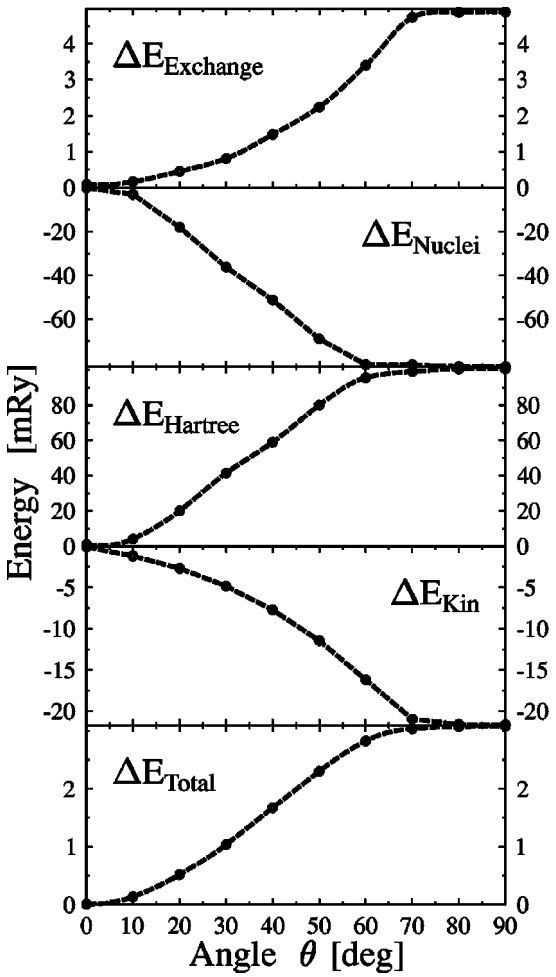

FIG. 2. Individual contributions to spin spiral formation energies $\Delta E(\theta)$ at $\boldsymbol{q}=(0,0,1)[\pi/a]$ for fcc-Ni. ΔE is defined as in Fig. 1. The contributions shown are: the SDFT exchange and correlation energy labeled E_{Exchange}, the electron-nuclei Coulomb energy labeled E_{Nuclei}, the Hartree energy of all electrons labeled E_{Hartree}, and the SDFT kinetic energy labeled E_{Kin}. The total of all contributions is labeled E_{Total}.

tially the exchange and correlation energy with a slight reduction by both kinetic and Coulomb energy for larger θ values, due to a slight expansion of the d shell when the moment is reduced. It shows again that this latter intraatomic energy balance contributes little to the interatomic magnetic interaction as long as not both $\boldsymbol{q}$ and θ are large. This gives further support to our central assumption (2.21).

B. Adiabatic magnon spectra

The computed magnon spectra of bcc-Fe, fcc-Co, and fcc-Ni are shown in Figs. 3–5. For a Bravais lattice there is only one (transversal) branch, and hence there is no eigenvalue problem left to solve in Eq. (2.30). One simply has

$$\omega_{\boldsymbol{q}}=\frac{g\mu_{\mathrm{Bohr}}}{\hbar}\tilde{J}_{\boldsymbol{q}}M. \tag{3.2}$$

In the cases of Fe and Ni, where experimental parts of the spectra are available from the literature, the agreement is excellent in the long-wavelength region and even good for shorter wavelengths when not considering the interference of

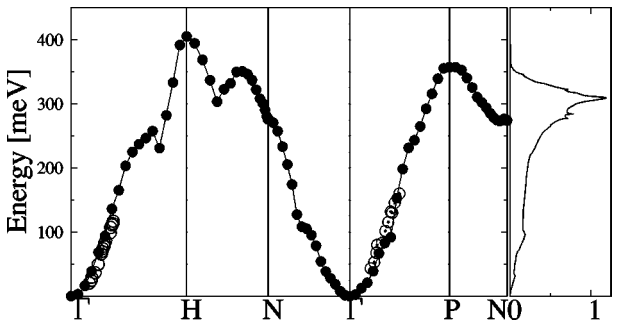

FIG. 3. Adiabatic magnon dispersion relations on high-symmetry lines and magnon densities of states [in states/(meV*cell)$\times 10^{-2}$] of bcc-Fe. Solid circles mark calculated frequencies, lines are guides for the eye. For comparison, experimental data, for pure Fe at 10 K: ⊙ Ref. 29, and for Fe (12%Si) at room temperature: ○ Ref. 30 are given. Note the Kohn anomalies (cusps) in the adiabatic spectrum.

a Stoner spin-flip excitation continuum around 150 meV in the case of Ni, which is not accounted for by our adiabatic approach. It may be obtained from a many-body treatment of the transverse magnetic susceptibility,[20] and it has sometimes been somewhat misleadingly called an ''optical magnon'' branch. Note that the results shown in Figs. 3–5 do not contain any adjustable parameter.

As an example with a true optical branch (at least in adiabatic treatment), we have also calculated the magnon spectrum of hcp-Co, which is shown in Fig. 4(b). Both the maximum frequency and the stiffness are not much different for fcc- and hcp-Co. However, the neglect of anisotropy terms in the adiabatic Hamiltonian is more problematic in the hcp case, where the true spectrum has a gap at zero frequency.

Note also that in all three metals the maximum adiabatic magnon frequency is roughly five times larger than the Curie temperature. Hence, high-$\boldsymbol{q}$ magnons seem to be sparsely occupied even close to the Curie temperature. We will come back to that point in Sec. IV.

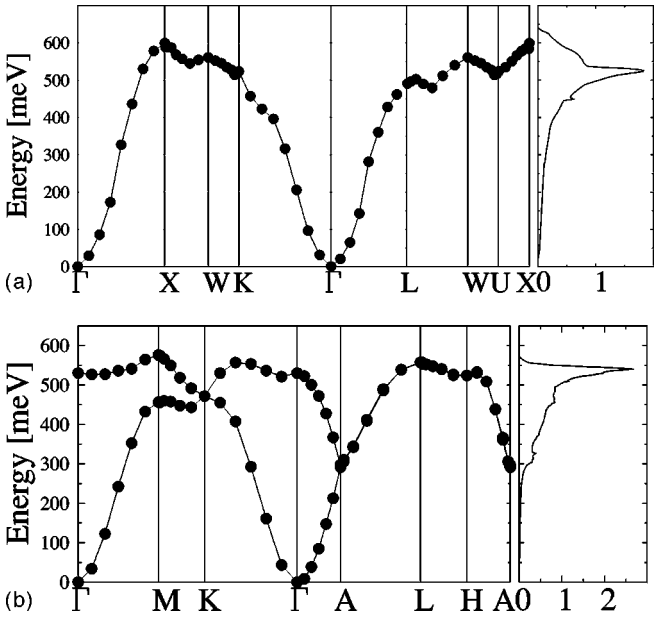

FIG. 4. As Fig. 3, but for (a) fcc Co, (b) hcp Co.

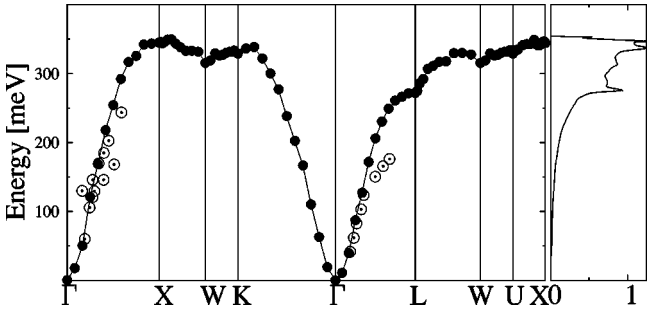

FIG. 5. As Fig. 3, but for fcc Ni. The experimental data (⊙) are those of Ref. 31.

C. Kohn anomalies

The direct SDFT calculation of the $\boldsymbol{q}$-dependent exchange constant matrix (2.18) via constrained spin spirals is capable of accounting for arbitrarily far reaching interactions. In analogy to phonon spectra, where in metals long-range interactions mediated by Friedel oscillations due to charge-density perturbations with Fermi-surface nesting vectors lead to Kohn-Migdal anomalies in the spectra, such anomalies at the same $\boldsymbol{q}$ positions and with the same cause are expected in the magnon spectra as anticipated already in the original paper by Kohn.[32]

The calculated adiabatic magnon spectra of Fe, displayed in Fig. 3, show prominent anomalies around point H and weaker ones in both Γ-N and Γ-P directions. In Fig. 6 we present Fermi-surface cross sections with symmetry planes for Fe, which indicate particularly strong nesting behavior of the majority-spin Fermi-surface pocket around Γ. Specifically, the plane part perpendicular to the Γ-H direction can explain the strong anomalies in the magnon dispersion around H both in Γ-H and H-N directions. Nesting behavior (small curvature) can also be assigned to some minority-spin Fermi-surface sheets, and they can be responsible for the weaker anomalies.

The study of the magnetic susceptibility in Ref. 20 indicates large windows free of spin-flip continua for Fe even at

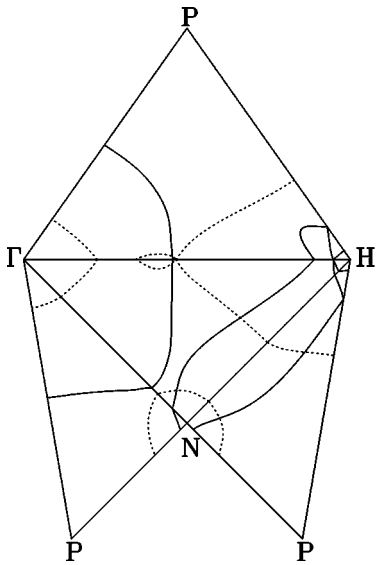

FIG. 6. Cross sections of the Fermi surface of Fe: solid lines: up spin, dashed lines: down spin. Note the considerable nesting behavior of the Γ-centered majority-spin Fermi-surface pocket.

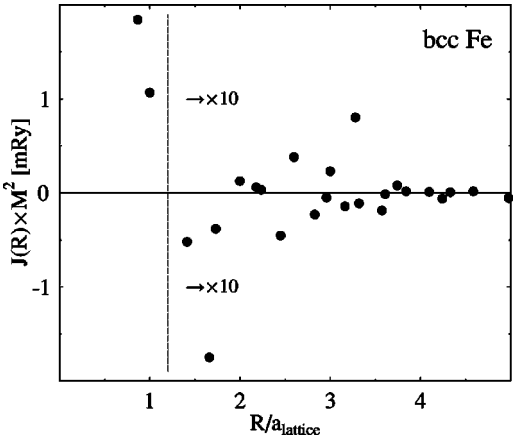

FIG. 7. Exchange constants J_{ij} of Fe as a function of neighbor distance R_{ij}. Note the oscillating behavior up to beyond 15 neighbors.

higher excitation energies, but lacking theoretical predictions, no particular experimental search for Kohn anomalies has been undertaken up to now, although several investigations of the high-energy magnetic excitation spectrum were reported.[29,33] Although the statistics are obviously not good enough, the experimental points along the line Γ-P of Fig. 3 are not unlikely to show the anomaly. More precise measurements in this area are strongly encouraged by our results.

In Fig. 7 the dependence of J_{ij}, which is obtained from Eqs. (2.14) and (2.18) as

$$J_{ij}=-\frac{V_{\mathrm{u.c.}}}{(2\pi)^3}\int_{\mathrm{BZ}} d^3q\, e^{-i\boldsymbol{q}\cdot(\boldsymbol{R}_i-\boldsymbol{R}_j)}\tilde{J}^{\mu_i\nu_j}_{\boldsymbol{q}}, \quad i\neq j, \quad (3.3)$$

on the site distance R_{ij} for Fe is displayed, demonstrating that there is indeed an oscillating long-range exchange interaction reaching beyond the 15th neighbor in the crystal. The constrained spin spiral approach seems to be, at present, the only technique to trace, quantitatively, such long-range exchange interactions.

IV. THERMAL EXCITATION OF MAGNONS AND PHASE DIAGRAM

Magnons should, in three dimensions, be expected to be the appropriate thermal magnetic excitations of magnetically polarized materials at low temperatures T. The results of the last section encouraged us to follow this idea. As long as the magnon-magnon interaction can be neglected, that is in the harmonic regime, the average mode amplitude $\langle\theta^2_{\nu\boldsymbol{q}n}\rangle$ is obtained by putting the mode energy (2.32) equal to $\hbar\omega_{\boldsymbol{q}n}n_{\boldsymbol{q}n}(T)$ in accordance with the Planck distribution

$$n_{\boldsymbol{q}n}(T)=\frac{1}{\exp(\hbar\omega_{\boldsymbol{q}n}/k_BT)-1}. \quad (4.1)$$

The same reasoning that led to Eq. (2.33) now results in

$$\frac{N}{2g\mu_{\mathrm{Bohr}}}\sum_{\mu} M_\mu\langle\theta^2_{\mu\boldsymbol{q}n}\rangle=n_{\boldsymbol{q}n}, \quad (4.2)$$

and the thermal reduction of the average sublattice magnetization is obtained as

$$\Delta M_\mu^z = M_\mu \sum_{\boldsymbol{q}n} [1-\langle \cos\theta_{\mu\boldsymbol{q}n}\rangle] \approx \frac{M_\mu}{2}\sum_{\boldsymbol{q}n} \langle \theta_{\mu\boldsymbol{q}n}^2\rangle. \quad (4.3)$$

Angular brackets denote thermal averaging in this section, which comprises averaging over the slow magnetic dynamics. Summation of Eq. (4.3) over μ and consideration of Eq. (4.2) as well as $(1/N)\Sigma_{\boldsymbol{q}} = [V_{\text{u.c.}}/(2\pi)^3]\int d^3q$ yields

$$\Delta M^z = \sum_\mu \Delta M_\mu^z = g\mu_{\text{Bohr}} \sum_n \frac{V_{\text{u.c.}}}{(2\pi)^3}\int_{\text{BZ}} d^3q\, n_{\boldsymbol{q}n} \quad (4.4)$$

for the thermal reduction of the average total magnetization.

Note that the adiabatic moments have already been subject to a quantum average over the fast electronic motion and hence are no longer quantum angular momentum operators. Consequently, they are also no longer subject to zero-point quantum fluctuations which reduce the z component of a quantum spin S from $\hbar[S(S+1)]^{1/2}$ to $\leqslant \hbar S$. The equations of motion (2.25) are already the quantum average of Eq. (2.24) and do not yield zero-point motion which was already averaged out in Eq. (2.21). This point is evocative to caution in using the adiabatic approach and, in particular, Eq. (2.21): for instance, it will probably not work for very weak magnetic materials.

At elevated temperature the occupation numbers and hence the amplitudes $\langle \theta_{\mu\boldsymbol{q}n}\rangle$ of long-wavelength modes become large. The modes start to interact both kinematically (deviation from bosonic character) and anharmonically, and finally the magnon picture is to be replaced by a picture of strong long-wavelength transverse spin fluctuations. In 3d metals, the $(T=0)$ magnon energies for $\boldsymbol{q}$ vectors close to the Brillouin-zone boundary are much higher than k_BT_C, the thermal energy at the Curie temperature, and hence spin clusters of many atoms are expected to be aligned even at the Curie temperature. Figure 1 then suggests that longitudinal spin fluctuations may be neglected even up to T_C. We therefore divide the temperature scale into two parts: the harmonic regime, roughly $T \lesssim T_C/2$, with well-defined quantum excitations, and the anharmonic regime, roughly $T_C/2 \lesssim T \lesssim T_C$, where one may call on semiclassical averaging schemes for the mean-field free energy as in Ref. 10, or, since longitudinal spin fluctuations seem to be negligible and the aligned clusters still seem to be mesoscopic, resort to the Langevin approach with an effective Weiss field

$$\boldsymbol{B}_{\text{Weiss}}^\nu = \sum_{\mu,\boldsymbol{R}}{}' J_{\nu[\mu+\boldsymbol{R}]}\langle \boldsymbol{M}_\mu\rangle = \sum_\mu J_0^{\nu\mu}\langle \boldsymbol{M}_\mu\rangle \quad (4.5)$$

acting on the moment $\boldsymbol{M}_\nu$ at a site of the sublattice ν and causing a thermally averaged sublattice polarization

$$\langle M_\nu\rangle = M_\nu \coth\left[\frac{M_\nu B_{\text{Weiss}}^\nu}{k_BT}\right] - \frac{k_BT}{B_{\text{Weiss}}^\nu} \quad (4.6)$$

in the direction of $\boldsymbol{B}_{\text{Weiss}}^\nu$. The prime on the sum of Eq. (4.5) means omission of a possible on-site term (for $\mu=\nu$), and from Eq. (3.3) one finds

$$J_0^{\nu\mu} = -\tilde{J}_{\boldsymbol{q}=0}^{\nu\mu} + \delta_{\nu\mu}\frac{V_{\text{u.c.}}}{(2\pi)^3}\int_{\text{BZ}} d^3q\, \tilde{J}_{\boldsymbol{q}}^{\nu\mu} e^{-i\boldsymbol{q}\cdot(\boldsymbol{\tau}_\nu-\boldsymbol{\tau}_\mu)}. \quad (4.7)$$

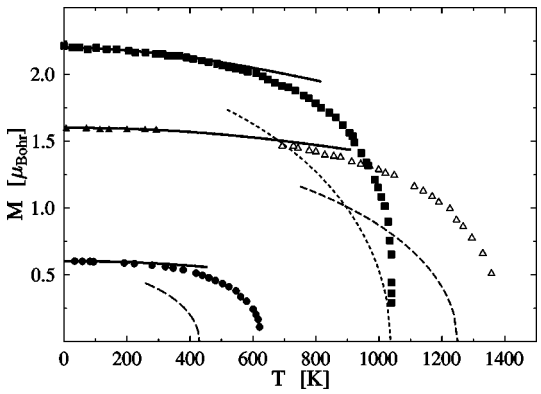

FIG. 8. Magnetization vs temperature of Fe [squares (Ref. 34)], Co [full triangles hcp (Ref. 35), open triangles fcc (Ref. 34)], and Ni [balls (Ref. 36)]. Solid lines: calculated from magnon spectra. Dashed lines: mean-field results.

For temperatures for which Eq. (4.6) has a nonzero solution, the material is magnetically ordered and the thermal average of the total magnetization (moment per unit cell) is now obtained by summation of Eq. (4.6) over ν. This approach assumes that on the fast time scale the site moment M_μ is practically temperature independent up to T_C. The Langevin formula is used because, again, this site moment is already a quantum average and hence may vary continuously.

In Fig. 8 the magnetization of 3d ferromagnets vs temperature T calculated according to Eqs. (4.4) and (4.6) for $T \lesssim T_C/2$ and $T_C/2 \lesssim T \lesssim T_C$, respectively, is compared with experimental values. (In Ref. 17 the mean-field part for Ni was rescaled.) In particular, the very satisfactory agreement between our calculation and experiment at low temperatures is due to our correct use of the Planck distribution of magnons instead of the semiclassical averaging of Ref. 10. It indicates that the low-temperature excitation spectrum is indeed well represented by magnons. The mean-field treatment for higher temperatures is only semiquantitatively correct.

Within this mean-field treatment, the Curie temperature itself is obtained as the boundary of the solubility of Eq. (4.6). This is the temperature at which the Weiss field vanishes, and therefore Eq. (4.6) may be replaced by the lowest order of an expansion in powers of $(M_\nu B_{\text{Weiss}}^\nu/k_BT)$ for $T \approx T_C$:

$$\langle M_\nu\rangle = \frac{M_\nu^2}{3k_BT}B_{\text{Weiss}}^\nu = \frac{M_\nu^2}{3k_BT}\sum_\mu J_0^{\nu\mu}\langle M_\mu\rangle. \quad (4.8)$$

The solubility condition of this homogeneous linear equation system for $\langle M\rangle$ is

$$\det\left(\delta_{\nu\mu} - \frac{M_\nu^2}{3k_BT_C}J_0^{\nu\mu}\right) = 0, \quad (4.9)$$

which simplifies for a Bravais lattice to the well-known expression

$$T_C = \frac{M^2J_0}{3k_B} \quad (4.10)$$

for the classical Langevin situation.

Our calculated Curie temperatures together with experimental values and with other theoretical estimates from the

TABLE I. Curie temperatures of bcc-Fe, hcp-Co, and fcc-Ni in Kelvin.

	T_C, present	T_C (Ref. 37)	T_C (Ref. 9)	T_C (Ref. 10)	T_C, Expt. (Ref. 38)
bcc Fe	1037	1270	1015	1095	1043
fcc Co	1250	1520		1012	1388
fcc Ni	430		450	412	627

literature are given in Table I. Probably the first SDFT calculation of Curie temperatures of 3*d* metals on the basis of Eq. (4.10) was reported in Ref. 39. However, these authors doubted the applicability of the Langevin expression and qualified the closeness to experimental values to some extent as a matter of chance. The deviation between the calculated Curie temperatures of Refs. 39 and 37 and ours is most probably due to differences in the calculation of J_0, where those authors summed over a finite number of neighbors in real space rather than our Fourier space treatment. Interestingly enough, a recent improvement[9] of the Korringa-Kohn-Rostoker coherent-potential-approximation approach[8] to the paramagnetic phase above T_C, which is based on similar adiabaticity assumptions, resulted in T_C values very close to ours.

We stress once more that due to our analysis, in particular the results of Fig. 1 in connection with the magnon energy scale related to T_C, the site moments remain fully developed on the fast time scale even above the Curie temperature. This relates nicely to very recent experimental findings[40] of strong short-range ferromagnetic correlations in magnetic neutron-scattering results for fcc-Fe-Ni alloys at high temperatures far above ordering temperatures and even for concentrations ($\sim$20% Ni) where there is practically no low-temperature magnetic order. On average, over the slow time scale there is of course no moment.

V. CONCLUDING REMARKS

The adiabatic treatment of the magnetic moment dynamics in itinerant magnets considers two time scales: a fast scale for the electronic motion comprising longitudinal spin fluctuations (as, e.g., Stoner excitations), and a slow scale for the transversal moment motion. The force constants (exchange constants) governing the latter motion are obtained from SDFT calculations for small amplitude spin spirals only. The low-energy excitations of bcc-Fe, Co, and fcc Ni are well described as adiabatic magnons displaying Kohn anomalies in case of Fermi-surface nesting and obeying Planck statistics. On the short time scale the site moments are stable even through the magnetic order transition. From the stiffness at $T=0$ in relation to $k_B T_C$, one may conjecture that large $\boldsymbol{q}$ modes are sparsely occupied even at T_C, and hence the ordered moment lattice melts into clusters of a few atomic distances in diameter in these metals. The individual site moments themselves are already on-site quantum averaged quantities and move quasiclassically at elevated temperature. Hence the Langevin free energy is the correct mean-field basis for the description of thermal behavior at elevated temperature.

ACKNOWLEDGMENTS

This work was supported financially by the Max-Planck Institute for Physics of Complex Systems and by the Max-Planck Research Unit Electron Systems, both at Dresden, as well as by the State of Saxony under Contract No. 4-7541.82-MP2/502. Discussions with Dr. M. Richter are kindly acknowledged.

*Permanent address: Institute for Metal Physics, Kiev, Ukraine.

[1] V. L. Moruzzi and P. Marcus, in *Handbook of Magnetic Materials*, edited by K. H. J. Buschow (Elsevier Science, New York 1993), p. 97.

[2] M. S. S. Brooks and B. Johansson, in *Handbook of Magnetic Materials* (Ref. 1), p. 139.

[3] Jun-Hyung Cho and M. Scheffler, Phys. Rev. B **53**, 10 685 (1996).

[4] L. M. Sandratskii, Phys. Status Solidi B **136**, 167 (1986).

[5] J. Kübler, K.-H. Höck, J. Sticht, and A. R. Williams, J. Phys. F **18**, 469 (1988).

[6] T. Oguchi, K. Terakura, and M. Hamada, J. Phys. F **13**, 145 (1983).

[7] A. J. Pindor, J. Staunton, G. M. Stocks, and H. Winter, J. Phys. F **13**, 979 (1983).

[8] B. L. Gyorffy, A. J. Pindor, J. B. Staunton, G. M. Stocks, and H. Winter, J. Phys. F **15**, 1337 (1985).

[9] J. B. Staunton and B. L. Gyorffy, Phys. Rev. Lett. **69**, 371 (1992).

[10] M. Uhl and J. Kübler, Phys. Rev. Lett. **77**, 334 (1996).

[11] N. M. Rosengaard and B. Johansson, Phys. Rev. B **55**, 14 975 (1997).

[12] V. P. Antropov, M. I. Katsnelson, M. van Schilfgaarde, and B. N. Harmon, Phys. Rev. Lett. **75**, 729 (1995).

[13] V. P. Antropov, M. I. Katsnelson, B. N. Harmon, M. van Schilfgaarde, and D. Kuznecov, Phys. Rev. B **54**, 1019 (1996).

[14] S. Akbar, Y. Kakehashi, and N. Kimura, J. Appl. Phys. **81**, 3862 (1997).

[15] T. Moriya, *Spin Fluctuations in Itinerant Electron Magnetism* (Springer, Berlin, 1985).

[16] H. Capellmann, *Metallic Magnetism* (Springer, Berlin, 1987).

[17] S. V. Halilov, A. Y. Perlov, P. M. Oppeneer, and H. Eschrig, Europhys. Lett. **39**, 91 (1997).

[18] J. F. Cooke, J. W. Lynn, and H. L. Davis, Phys. Rev. B **21**, 4118 (1980).

[19] J. Callaway, A. K. Chatterjee, S. P. Singhal, and A. Ziegler, Phys. Rev. B **28**, 3818 (1983).

[20] J. F. Cooke, J. A. Blackman, and T. Morgan, Phys. Rev. Lett. **54**, 718 (1985).

[21] J. A. Blackman, T. Morgan, and J. F. Cooke, Phys. Rev. Lett. **55**, 2814 (1985).
[22] E. Stenzel and H. Winter, J. Phys. F **16**, 1789 (1986).
[23] L. M. Sandratskii, J. Phys.: Condens. Matter **3**, 8565 (1991); W. Brinkman and R. J. Elliott, Proc. R. Soc. London, Ser. A **294**, 343 (1966).
[24] O. K. Andersen, Phys. Rev. B **12**, 3060 (1975).
[25] H. L. Skriver, *The LMTO Method* (Springer, Berlin, 1984), § 9.6.
[26] U. von Barth and L. Hedin, J. Phys. C **5**, 1629 (1972).
[27] J. Hubbard, Phys. Rev. B **19**, 2626 (1979); *ibid.* **20**, 4584 (1979); J. Appl. Phys. **52**, 1654 (1981).
[28] M. V. You, V. Heine, A. J. Holden, P. J. Lin-Chung, Phys. Rev. Lett. **44**, 1282 (1980).
[29] C.-K. Loong, J. M. Carpenter, J. W. Lynn, R. A. Robinson, and H. A. Mook, J. Appl. Phys. **55**, 1895 (1984).
[30] J. W. Lynn, Phys. Rev. B **11**, 2624 (1975).
[31] H. A. Mook and D. McK. Paul, Phys. Rev. Lett. **54**, 227 (1985).
[32] W. Kohn, Phys. Rev. Lett. **2**, 393 (1959).
[33] T. G. Perring, A. T. Boothroyd, D. McK. Paul, A. D. Taylor, R. Osborn, R. J. Newport, J. A. Blackman, and H. A. Mook, J. Appl. Phys. **69**, 6219 (1991); M. Yethiraj, R. A. Robinson, D. S. Sivia, J. W. Lynn, and H. A. Mook, Phys. Rev. B **43**, 2565 (1991); A. T. Boothroyd, T. G. Perring, A. D. Taylor, D. McK. Paul, and H. A. Mook, J. Magn. Magn. Mater. **104-107**, 713 (1992).
[34] J. Crangle and G. M. Goodman, Proc. R. Soc. London, Ser. A **321**, 477 (1971).
[35] R. Pauthenet, J. Appl. Phys. **53**, 2029 (1982).
[36] P. Weiss and R. Forrer, Ann. Phys. (Leipzig) **5**, 153 (1926).
[37] R. F. Sabiryanov, S. K. Bose, and O. N. Mryasov, Phys. Rev. B **51**, 8958 (1995).
[38] N. W. Ashcroft and N. D. Mermin, *Solid State Physics* (Holt, Rinehart and Winston, New York, 1976).
[39] A. I. Liechtenstein, M. I. Katsnelson, V. P. Antropov, and V. A. Gubanov, J. Magn. Magn. Mater. **67**, 65 (1987).
[40] M. Acet, E. F. Wassermann, K. Andersen, A. Murani, and O. Schärpff, Europhys. Lett. **40**, 93 (1997).